Pasquier, R., D'Angelo, L., Goulet, J., Acevedo, C., Nussbaumer, A. and Smith, I.F.C: (2016). "Measurement, Data Interpretation, and Uncertainty Propagation for Fatigue Assessments of Structures." Journal of Bridge Engineering, 10.1061/(ASCE)BE.1943-5592.0000861, 04015087. http://cedb.asce.org Copyright ASCE

Measurement, data interpretation and uncertainty propagation for fatigue assessments of structures

Romain Pasquier, S. M. ASCE[1] ; Luca D'Angelo[2] ; James-A. Goulet[3]

Claire Acevedo[4] ; Alain Nussbaumer[5] and Ian F. C. Smith, F. ASCE[6]

Abstract

Real behavior of existing structures is usually associated with large uncertainty that is often covered by the use of conservative models and code practices for the evaluation of remaining fatigue lives. In order to make better decisions related to retrofit and replacement of existing bridges, new techniques that are able to quantify fatigue reserve capacity are required. This paper presents a population-based prognosis methodology that takes advantage of in-service behavior measurements using model-based data interpretation. This approach is combined with advanced traffic and fatigue models to refine remaining-fatigue-life predictions. The study of a full-scale bridge demonstrates that this methodology provides less conservative estimations of remaining fatigue lives. In addition, this approach propagates uncertainties associated with finite-element, traffic and fatigue-damage models to quantify their effects on fatigue-damage assessments and shows that traffic models and structural model parameters are the most influential sources of uncertainty.

Keywords: Modeling uncertainty, behavior measurement, model-based data interpretation, traffic-load model, hot-spot stress.

[1]Ph.D Student, Applied Computing and Mechanics Laboratory (IMAC), School of Architecture, Civil and Environmental Engineering (ENAC), Swiss Federal Institute of Technology (EPFL), CH-1015 Lausanne, Switzerland (corresponding author). Email address: rpasquie@gmail.com

[2]Ph.D Student, Steel Structures Laboratory (ICOM), School of Architecture, Civil and Environmental Engineering (ENAC), Swiss Federal Institute of Technology (EPFL), CH-1015 Lausanne, Switzerland

[3]Fellow Postdoctoral Researcher, Department of Civil and Environmental Engineering, University of California, Berkeley, CA 94720, USA

[4]Fellow Postdoctoral Researcher, Materials Sciences Division, Lawrence Berkeley National Laboratory, Berkeley, CA 94720, and Department of Materials Science and Engineering, University of California, Berkeley, CA 94720, USA

[5]Professor, Steel Structures Laboratory (ICOM), School of Architecture, Civil and Environmental Engineering (ENAC), Swiss Federal Institute of Technology (EPFL), CH-1015 Lausanne, Switzerland

[6]Professor, Applied Computing and Mechanics Laboratory (IMAC), School of Architecture, Civil and Environmental Engineering (ENAC), Swiss Federal Institute of Technology (EPFL), CH-1015 Lausanne, Switzerland

INTRODUCTION

Due to the uncertainty associated with real behavior of existing structures, conservative models and code practices are often used to evaluate remaining lives. However, the increasing importance of economic and environmental issues related to retrofit and replacement of existing structures has led to the need for new techniques that are able to refine evaluations reserve capacity. For the case of fatigue evaluations of existing steel bridges, weigh-in-motion data and probabilistic tools can now improve traffic-load models. Also, advances in fatigue-damage models of complex connections are able to enhance the estimation of remaining fatigue life. In order to leverage such techniques, model-based data interpretation approaches are required to identify physics-based models that are capable of accurately predicting structural behavior. Behavior measurements (e.g., displacements, tilts, strains and accelerations) are thus needed to identify unknown physical parameters of such models and reduce uncertainties associated with predictions.

Several studies have performed fatigue assessments using direct measurements that provide accurate estimations of stress-ranges occurring during monitoring and using various fatigue-damage models (Sweeney 1976; Li et al. 2001; Zhou 2006; Soliman et al. 2013; Kwon et al. 2013). However, this information typically falls short when extrapolated for other locations and for other load configurations. In practical applications, models are required to predict quantities that are not measured directly due to a range of technological, economic and practical reasons. Extrapolation is feasible using indirect behavior measurements and physics-based models, such as finite-element models. In addition, inferring the correct values of physical parameters is essential for understanding the true behavior of structures and for enhancing confidence in model extrapolation (Farajpour and Atamturktur 2012; Brynjarsdóttir and O'Hagan 2014).

Many studies have used behavior models to make fatigue assessments of structures using traffic simulations (Leander et al. 2010; Leitão et al. 2011; Guo et al. 2012) and advanced fatigue-damage models (Siriwardane et al. 2008; Liu et al. 2010). However, these models have been either validated or calibrated without accounting for modeling and measurement uncertainties. Verification of compatibility of behavior models with measurements does not guarantee accurate predictions,

particularly in the presence of systematic modeling uncertainties that are unavoidable when idealizing complex systems. Model-based data-interpretation techniques that include modeling and measurement uncertainties are required in order to infer unknown structural properties, thereby improving fatigue assessments (prognosis).

Model-based data interpretation for complex systems is an ambiguous task that usually leads to multiple explannations for measured behavior. Thus, model-based data-interpretation approaches leading to a single calibrated model offer limited support for decisions and prognosis (Beven 2006; Neumann and Gujer 2008; Beck 2010; Goulet and Smith 2013; Atamturktur et al. 2014). Probabilistic techniques such as Bayesian inference (Mackay 2003; Yuen 2010) are available for updating the knowledge of model parameters and accommodating multiple solutions. Many examples have been reported where Bayesian methodologies lead to correct parameter identification and extrapolations in situations where information is available for defining the joint probability density function (PDF) of modeling and measurement errors and where systematic errors are absent (Beck and Katafygiotis 1998; Papadimitriou et al. 2001; Beck and Au 2002; Zhang et al. 2013). However, systematic errors are common when modeling complex structures, due to simplifications and omissions made in the process of idealization. Goulet and Smith (2013) have proposed a population-based data interpretation technique called error-domain model falsification (EDMF). This methodology is most appropriate for performing diagnosis when knowledge of errors is incomplete.

Proper consideration of traffic induced loadings is a technical challenge in the fatigue life assessment of road bridges. Traffic-load models that are proposed in codes (AASHTO 2007; EN1993-1-9 2005; SIA261 Code 2003) can return errors in the calculation of loading stress-range spectra resulting in significant errors in remaining-fatigue-life estimations. In addition, local load spectrum often varies significantly from the national average (Moses et al. 1987). The combination of the weigh-in-motion (WIM) technique with traffic simulation provides a solution to this challenge. This technique allows for integrating traffic-loading uncertainties in the fatigue-damage assessment. Several studies have used this approach for building suitable traffic-load models

(Crespo-Minguillón and Casas 1997; Leahy et al. 2014; Morales-Nápoles and Steenbergen 2015). However, no study have been found where traffic simulations and population of finite-element models obtained using data interpretation are combined in order to estimate remaining fatigue lives of structures.

Pasquier et al. (2014) proposed a population-based prognosis methodology based on error-domain model falsification and code practices that is able to refine remaining-fatigue-life predictions by taking advantage of in-service behavior measurements. A case study on a hollow-section truss bridge has demonstrated that this approach is able to reduce uncertainty associated with remaining-fatigue-life predictions. However, the fatigue-damage assessment of hollow section joints has been carried out based only on simplified fatigue models.

Due to the complexity of the stress field in hollow section joints, the hot-spot stress method, also known as the geometric stress method, is employed to evaluate the fatigue life of bridges made of tubular elements. This method provides $\mathrm{S_{rhs}}$-N curves based on experimental data where the $\mathrm{S_{rhs}}$ relates to the hot-spot stress range in that joint, rather than the nominal stress range used in the conventional fatigue classification method (Maddox 1997; Niemi et al. 2006). The hot-spot stress is extrapolated at the weld toe, where potential crack initiation sites (hot spots) are expected. Contrary to the nominal stress, the hot-spot stress includes the effect of the joint geometry (stress concentration), the type of load and the weld shape being idealized. Therefore, the $\mathrm{S_{rhs}}$-N curve presents the advantage of simplifying $\mathrm{S_{nom}}$-N curves given for each detail category into single design curve depending on weld type by including the global detail geometry in the hot-spot stress calculation (Hobbacher 2007).

This paper builds on the work by Pasquier et al. (2014) and enhances the population-based prognosis methodology by combining advanced traffic and fatigue models with on-site behavior measurements in order to further improve predictions of remaining fatigue lives. By propagating uncertainties associated with these advanced strategies, the methodology provides insight into sources of uncertainty for the prediction of fatigue-reserve capacity as well as support for management decisions related to structural retrofit, repair and replacement. The first section describes

the enhanced prognosis methodology and the second section presents a full-scale case study that illustrates the overall benefits of the approach.

POPULATION-BASED FATIGUE PROGNOSIS

This section describes the population-based prognosis methodology for remaining-fatigue-life evaluation of tubular K-joints in existing bridges. First, error-domain model falsification, the system-identification approach, is presented. Then, the second section explains the process of influence-line predictions based on models identified by EDMF. Traffic simulations based on WIM data and the hot-spot stress method for tubular K-joints are then described. Finally, the last section explains how uncertainty is propagated throughout the methodology in order to predict the remaining fatigue life and how the uncertainty relative importance is determined. Also in this section, a flowchart summarizing the methodology is presented in Figure 3.

Error-domain model falsification

The goal of *system identification* is to combine the information provided by model predictions and by measurements in order to learn what are possible values for $\boldsymbol{\theta}$, which describe characteristic properties of a structure. Estimates for n_Y *characteristic responses* Y_i of a structure can be provided by models as well as by in-situ observations of a constructed system. Let $g_i^{\{m\}}(\boldsymbol{\theta})$ denote model predictions from a model class $\{m\}$ and taking as input a set of parameter values $\boldsymbol{\theta}$, $\hat{y}_i$ denotes observations, and $\{U_{i,g},\ U_{i,\hat{y}}\}$ respectively denotes a random variable describing model prediction and measurement errors for the i^{th} structural characteristic response. In this paper, the superscript $\{m\}$ denoting the model class is omitted in order to simplify the notation. The relationships between a characteristic response and a model prediction is given by

$$Y_i = g_i(\boldsymbol{\theta}) + U_{i,g}, \quad \forall i = 1, 2, \ldots, n_Y \tag{1}$$

and between a characteristic response and a measurement is

$$Y_i = \hat{y}_i + U_{i,\hat{y}}, \quad \forall i = 1, 2, \ldots, n_Y \tag{2}$$

The joint probability density function (PDF) $f_{\mathbf{U}_{\hat{y}}}(\mathbf{u}_{\hat{y}})$ describing the measurement error is in common cases estimated from repeated calibration experiments performed in controlled conditions. In the case of civil structures, such a characterization is usually not possible for the joint PDF of model-prediction errors, $f_{\mathbf{U}_g}(\mathbf{u}_g)$; instead, $f_{\mathbf{U}_g}(\mathbf{u}_g)$ is commonly estimated based on heuristics and expert knowledge. Examples of sources of modeling uncertainty are idealized support and connection conditions, weld geometry, temperature effects, load amplitude and load position, Bernoulli-beam hypothesis, geometric variability of the structure, constitutive law of materials, etc. For finite-element models, examples are also mesh refinement and interpolation, element-type choices, the presence of singularities, etc. Because modeling uncertainty associated with complex systems commonly has a larger variance than measurement uncertainty, the joint PDF describing the combination of modeling and measurement uncertainties, $f_{\mathbf{U}_\mathrm{c}}(\mathbf{u}_\mathrm{c}) \sim \mathbf{U}_{\hat{y}} - \mathbf{U}_g$ is also dominated by heuristics and expert knowledge.

Error-domain model falsification performs system identification by generating an initial population of model instances $\{\boldsymbol{\theta}_k\},\ k = 1, 2, \cdots, n_k$ and then falsifies those instances that are not compatible with observations given modeling and measurement uncertainties. The candidate model set Ω consists in the initial model set minus the falsified models so that

$$\Omega = \{k : T_{i,\text{low}} \leq g_i(\boldsymbol{\theta}_k) - \hat{y}_i \leq T_{i,\text{high}}, \forall i\} \tag{3}$$

where $T_{i,\text{low}}$ and $T_{i,\text{high}}$ are threshold bounds defining the shortest intervals including a probability ϕ_d^{1/n_Y} for the marginal PDFs of $f_{\mathbf{U}_\mathrm{c}}(\mathbf{u}_\mathrm{c})$, where $\phi_d \in [0, 1]$ is the target reliability usually set at 0.95.

Influence-line prediction

The population-based fatigue prognosis methodology predicts remaining fatigue lives using candidate models obtained as described in the first section, traffic simulations and hot-spot stress-range calculations. For the determination of hot-spot stresses of a welded K-joint, internal forces of members (braces (br) and chord (ch)) are required to calculate nominal stresses (axial (ax) and

in-plane-bending (ipb) stresses) acting in the joint. In order to lower the effects of local stress concentrations, internal forces are extracted at a distance $\delta = 1.9 \cdot D$ and $\delta = 2.2 \cdot d$ of the joint (Schumacher et al. 2003), with D and d being the chord and the brace outer diameters. Axial forces N, in-plane-bending moments M and also shear-forces V are extracted at each of the four members of the joint such that in-plane-bending stresses at the joint are calculated using the shear-force linear variation. Figure 1 illustrates the internal forces and the nominal stresses involved in the calculation of hot-spot stresses.

The knowledge of internal forces in a bridge is based on load models that represent heavy-vehicle traffic crossing the structure. To be able to perform traffic simulations, influence lines of internal forces acting at critical joints are required. These influence lines are predicted using the candidate models and a moving reference axle load.

Each point of the influence line of an internal force $Q_j(x_l)$ for n_j locations is obtained using Eq. (4), where x_l is the location of the axle loading on the bridge.

$$Q_j(x_l) = g_j(x_l, \boldsymbol{\theta}_K) + U_{j,g}(x_l), \quad \forall j = 1, 2, \ldots, n_j \tag{4}$$

In Eq. (4), the candidate models are randomly selected using a discrete random variable K that is defined by the PDF:

$$f_K(k) = \begin{cases} 1/\#\Omega, & \forall k \in \Omega \\ 0, & otherwise \end{cases} \tag{5}$$

Thus, $Q_j(x_l)$ is a random variable described by a PDF obtained by the combination of internal-force prediction values for each candidate model $g_j(x_l, \boldsymbol{\theta}_K)$ and the distribution of modeling uncertainties, $U_{j,g}(x_l)$. Then, influence lines are used to generate the spectra of internal forces $N(t)$, $V(t)$ and $M(t)$ from a traffic model for each member of each critical joint.

Traffic model

In order to determine a realistic spectrum of internal forces, traffic of heavy vehicles crossing the bridge is modeled based on measured weigh-in-motion (WIM) data. WIM devices capture

static vehicle axle weights and provide information on: (1) vehicle arrival time (VAT); (2) vehicle speed (VS); (3) gross vehicle weight (GVW); (4) vehicle total length (TVL); (5) vehicle axle load (AVW); and (6) vehicle axle spacing (AVS). Only heavy vehicles with GVW larger than ten tons are taken into account since lighter vehicles lead to a negligible contribution to the bridge fatigue damage.

The traffic simulation tool takes as input the WIM raw data spreadsheet and classifies observed heavy vehicles in 13 classes according to *GR03-EUR13* classifications (Table A.2 (Meystre and Hirt 2006)). A mean value and a covariance matrix are assigned to the random variables GVW, TVL, AVW and AVS of each class based on WIM data. In addition, a normal PDF and a Burr PDF (Kleiber and Kotz 2003) are fitted to observed vehicle speeds (VS) and to observed inter-arrival times (VIT). Inter-arrival times are computed based on the difference between arrival times of consecutive vehicles. The distributions for VAT, VS, GVW, TVL, AVW and AVS represent the probabilistic traffic model. In order to determine the spectrum of internal forces $N(t)$, $V(t)$ and $M(t)$, a sequence of axle loadings (i.e. trucks being represented by either two or more axles with defined AVS) is randomly generated based on the traffic model for a representative traffic period. In this sequence, each axle loading refers to a time t. At each x_l along the bridge length, the generated axle loading of time t is superimposed to internal-force influence lines for determining $N(t)$, $V(t)$ and $M(t)$. Although the influence lines are determined based on a reference axle loading, the internal forces related to traffic simulation can be obtained by proportionality of axle-loading value since the bridge finite-element model behaves elastically. Thus, knowing the axle-load value of the traffic sequence and the reference axle-loading value, the internal forces are multiplied by the ratio of these values. This procedure is repeated for each time step of the sequence and the spectrum of internal forces is determined for a single lane. The random traffic sequences for different lanes are generated individually. Finally, the spectra of individual lanes are summed up to obtain the total internal-force spectrum at the critical joint members.

Hot-spot stress method

Knowing the spectrum internal forces ($N(t)$, $V(t)$ and $M(t)$) in the truss members at a distance δ of the joint enables calculation of the spectrum of axial and in-plane bending stresses at the weld toe (critical point). Axial stresses are constant along members between two joints, whereas in-plane-bending stresses vary linearly over the length of members. Therefore, spectra of nominal stresses in brace and chord members are generated from spectra of internal forces according to Eq. (6):

$$\begin{aligned} \sigma_{ax}(t) &= \frac{N(t)}{A} \\ \sigma_{ipb}(t) &= \frac{M(t) + V(t) \cdot \delta}{W} \end{aligned} \tag{6}$$

where A and W are the member cross-section area and the elastic section modulus, respectively, and δ is the distance from the weld toe to the position where the shear force V is extracted. At weld toes, where fatigue cracks are expected, geometrical discontinuities cause stress deviations and stress concentrations. This effect is taken into account in the calculation of hot-spot stresses $\sigma_{hs,i}$ by multiplying the member stress σ away from the joint by the stress concentration factor SCF_i as shown in Eq. (7):

$$\sigma_{hs,i} = \sigma \cdot SCF_i \tag{7}$$

where index i represents the hot-spot location.

Since stresses are elastic, the total hot-spot stress $\sigma_{hs,i}$ at hot spot i is the superposition of individual hot-spot stress under each load case (Zhao et al. 2000) and thus the hot-spot stress spectrum is calculated over time t as follows (axial brace force: $ax-br$, moment in brace: $ipb-br$, axial chord force: $ax-ch$, moment in chord: $ipb-ch$):

$$\begin{aligned} \sigma_{hs,i}(t) = \sigma_{ax-br}(t) \cdot SCF_{i,ax-br} + \sigma_{ipb-br}(t) \cdot (0.5 \cdot SCF_{i,ipb1-br} + 0.5 \cdot SCF_{i,ipb2-br}) \\ + \sigma_{ax-ch}(t) \cdot SCF_{i,ax-ch} + \sigma_{ipb-ch}(t) \cdot SCF_{i,ipb-ch} \end{aligned} \tag{8}$$

The stress concentration factors are determined from Schumacher et al. (2003) for K-joints

defined by geometric parameters $\beta = \frac{d}{D}$, $\gamma = \frac{D}{2T}$ and $\tau = \frac{t_{br}}{T}$ where d is the outer brace diameter, D is the outer chord diameter, t_{br} is the brace wall thickness and T is the chord wall thickness. Thus, spectra of hot-spot stresses are generated from spectra of nominal stresses and stress concentration factors at critical joint locations. In tubular K-joints, the most common crack location is encountered at hot spot 1 ($hs1$), which is situated at the weld toe in the chord, and for joints with tension in the chord, on the tension brace side (see Figure 2) (Acevedo and Nussbaumer 2012). This methodology, which expresses hot-spot stress spectrum from the nominal stress spectrum in Eq. (8), is more optimistic than expressing hot-spot stress ranges from nominal stress ranges. Indeed, computing the nominal stress ranges before using the hot-spot stress method leads to the loss of synchronicity of axial and in-plane-bending nominal stresses that appear in the traffic simulation. Such procedures lead to unnecessary conservatism in the hot-spot stress-range calculation since peaks in axial stresses and their ranges do not necessarily act at the same time as the peaks in in-plane-bending stresses. Thus, evaluating hot-spot stress spectra helps preserve the simultaneity of stress ranges acting at critical joints.

Remaining-fatigue-life prediction

Histograms of hot-spot stress ranges are obtained using the rainflow algorithm (Downing and Socie 1982) and are then compared to the $\mathrm{S_{rhs}}$-N curve referring to the joint category under study for the determination of the damage index. $\mathrm{S_{rhs}}$-N curves may be either provided by codes (SIA263 Code 2003; Zhao et al. 2000) or based on experimental data in order to avoid using deterministic values in this methodology. Provided that a sufficient number of experimental results are used, a regression model can be identified and then used for the comparison of stress ranges. The damage index $\mathcal{D}_{\mathrm{period}}$ is then computed using Miner's rule (Miner 1945) in Eq. (9) where damage induced by each stress range h of the histogram are summed for the period of traffic that is simulated.

$$\mathcal{D}_{\mathrm{period}} = \sum \frac{n_h}{N_h} = \sum \frac{n_h}{C \cdot \Delta\sigma_{hs,i,h}^{-m}} \tag{9}$$

In Eq. (9), the S_{rhs}-N curve is described by $C \cdot \Delta\sigma_{hs,i,h}^{-m}$, where C is a constant depending on the detail category and m is the slope coefficient; for steels, it is usually defined as $m = 3$. The remaining fatigue life RFL in years is then obtained using Eq. (10):

$$RFL = \frac{R_{\text{year}}}{\mathcal{D}_{\text{period}}} \tag{10}$$

where R_{year} is the portion of traffic simulation period over one year. For example, one week of traffic simulations is extrapolated in years using $R_{\text{year}} = 1/52$. In Eq. (10), traffic is assumed constant during the joint life and failure is assumed to occur when the damage index reaches unity.

Propagation of uncertainty and sensitivity analysis

In previous sections, Equations 6 through 10 have been written for a single model instance and a single critical joint. In the population-based prognosis methodology, N, V and M are random variables, $N_{br,j}(x_l)$,$V_{br,j}(x_l)$ and $M_{br,j}(x_l)$ and are obtained from Eq. (4) (here, for the brace internal forces of the j^{th} joint and similarly transposed for the chord internal forces). Using the probabilistic traffic model, random samples are generated from the distributions VAT, VS, GVW, TVL, AVW and AVS in order to define a random sequence of axle loadings. After traffic simulations, these internal forces are time dependent: $N_{br,j}(t)$,$V_{br,j}(t)$ and $M_{br,j}(t)$. Consecutively, axial and in-plane-bending stresses, hot-spot stresses and hot-spot stress ranges are random variables, $\sigma_{ax,j}(t)$, $\sigma_{ipb,j}(t)$, $\sigma_{hs,i,j}(t)$ and $\Delta\sigma_{hs,i,j}(t)$. Then, from Eq. (9), $\mathcal{D}_{\text{period}}$ becomes the random variable $\mathcal{D}_{\text{period},j}$ and similarly for RFL_j from Eq. (10).

Finally, using a number of samples n_{SP} of random variables in Eq. (4), the probability density function of RFL_j for the j^{th} joint among the n_j joint locations is obtained using Monte-Carlo analysis. For each Monte-Carlo step, the influence line of a candidate-model sample K is used to calculate the remaining fatigue life from a random traffic sequence and a random S_{rhs}-N curve sample. A sufficient number of samples n_{SP} should be generated in order to ensure convergence of the remaining-fatigue-life distribution. Using this process, model-parameter uncertainties, modeling uncertainties, traffic uncertainties and S_{rhs}-N curve uncertainty are propagated through remaining-

fatigue-life predictions. Lower and higher remaining-fatigue-life prediction thresholds are then evaluated for each distribution RFL_j. These thresholds represent the shortest interval including a target probability of prediction ϕ_p. Prediction thresholds are a robust representation of the remaining-fatigue-life uncertainty when little information is available for defining the true model of errors associated with remaining-fatigue-life values. Since the identification reliability is ϕ_d, and since the process involves independent random variables, the probability of having the true prediction value included between prediction thresholds for each critical joint independently is at least $\phi_d \cdot \phi_p$, given the estimated PDF of uncertainty.

Figure 3 summarizes the population-based prognosis methodology starting from the initial population of model instances to the remaining-fatigue-life prediction of a single critical joint. After falsification, n_{SP} candidate-model samples are used to predict influence lines of member internal forces including modeling uncertainties. Then, the damage index of each candidate-model sample is determined through a Monte-Carlo analysis over each n_{SP} samples using traffic simulations for computing internal-force spectra, nominal-stress spectra, hot-spot stress spectrum, rainflow analysis and $\mathrm{S_{rhs}}$-N curve comparison. Finally, from the damage index, the distribution of remaining-fatigue-life predictions is determined.

In this methodology, model-parameter uncertainties, modeling uncertainties, traffic uncertainties and $\mathrm{S_{rhs}}$-N curve uncertainty are propagated across the process of fatigue prognosis. In order to determine the relative importance of each uncertainty source involved in the process, a sensitivity analysis can be undertaken. Here, the sensitivity analysis is based on the response surface methodology (Box and Draper 1959; Fang et al. 2005). Let $\boldsymbol{Y} = f(X_1, X_2, \ldots, X_i, \ldots, X_n)$ be the response of a model f having random variables $\boldsymbol{X}$ as parameters. Variables $\boldsymbol{X}$ are used to build a model matrix $\boldsymbol{M}$ whose elements are standardized in the sense of design of experiments. The model f can be approximated by a linear function $\boldsymbol{Y} \approx \boldsymbol{M\beta}$, where $\boldsymbol{\beta}$ contains the parameters of the linear function. This expression can be solved using the least squares method such that:

$$\hat{\boldsymbol{\beta}} = (\boldsymbol{M^T M})^{-1}(\boldsymbol{M^T Y}) \tag{11}$$

where the vector $\hat{\boldsymbol{\beta}} = [\hat{\beta}_0, \hat{\beta}_1, \hat{\beta}_2, \ldots, \hat{\beta}_i, \ldots, \hat{\beta}_n]^T$ represents the least-square estimator of the true parameter vector and thus, whose elements represent the importance of each variable X_i on the response $\boldsymbol{Y}$, except $\hat{\beta}_0$ that is the constant term of the linear function. The relative importance of the random variables X_i is then computed over the sum of all importances: $\frac{\hat{\beta}_i}{\sum_{i=1}^{n} \hat{\beta}_i}$.

CASE STUDY: AARWANGEN BRIDGE

Structure description

The example under study is a composite-steel-concrete bridge over the Aar river and located in the city of Aarwangen (Switzerland). The bridge has two spans of 47.8 m with welded tubular steel trusses connected in a composite manner to the concrete deck that is 8.3 m wide. The cross-section of the finite-element model and its general overview are displayed in Figure 4. This bridge carries the bidirectional traffic with two lanes (west and east) of a main road going from Langenthal to an exit on the highway Bern-Zurich and Niederbipp. On average, $2,572$ trucks with an average weight of 18 tons cross the bridge in both directions every week.

The purpose of this study is to improve the reserve-capacity estimation of two K-joint connections of the truss as shown in Figure 5. Each K-joint has southern and northern welds, leading to four critical joints to evaluate overall. The failure location for these four joints is assumed in the chord (hot spot 1). This location is defined as the critical hot-spot position for this study in order to avoid the increase of complexity related to the evaluation of the other hot-spot locations.

The structure takes a set of six unknown parameter values $\boldsymbol{\theta} = [\theta_1, \theta_2, \ldots, \theta_6]$: the rotational stiffness of the truss connections, the longitudinal stiffnesses of the pavement covering expansion joints, and Young's moduli of steel, concrete and pavement. In the finite-element model, the connection stiffness and the southern and northern expansion-joint stiffnesses are modeled using rotational and longitudinal springs. These parameters are illustrated in Figure 6.

Model falsification and influence-line computation

As presented in Pasquier et al. (2014), the parameter values are identified using behavior measurements that are determined from static-load tests. From an initial population of $15,625$ model

instances, a subset of 69 candidate models are compatible with 21 strain measurements made during static-load testing (Pasquier et al. 2014) by following the error-domain model falsification approach using a target reliability $\phi_d = 0.95$.

The 69 candidate models are used to predict the influence lines of chord and brace internal forces for the two K-joints (overall 24 internal forces). A reference axle loading based on codes (SIA261 Code 2003) is used to compute the influence lines. The load moves from one end of the bridge to the other by step x_l of two meters, leading to overall $l = 49$ load steps. Influence lines are determined in turns for west and east lane axle loading.

The resolution of influence-line discretization obtained through finite-element analysis could be too low to be used for simulating traffic due to high demand in computing time for increasing the resolution. In such case, a linear interpolation is undertaken for increasing the influence-line resolution. The error associated with the interpolation is then quantified and combined with the other modeling uncertainties. For Aarwangen Bridge, since 49 load steps do not return a high enough influence-line resolution for the traffic-simulation process, a linear interpolation is carried out in order to obtain influence lines of 193 points. It would be computationally demanding, and not necessarily more accurate, to calculate influence lines of 193 points for each candidate model. In order to determine the error induced by the interpolated influence line, the influence line for 193 points is determined using the finite-element model for the model instance having the mean values of parameters $\overline{\boldsymbol{\theta}}$. Then, the interpolation errors for the 193 points are obtained by comparing this influence line with the interpolated one. The same procedure is carried out for the influence lines of modeling uncertainties. In this way, the interpolation error can be combined with the other modeling uncertainties at the 193 points.

Then, the distribution of influence lines of each internal force is determined using Eq. (4), including the interpolation error in the modeling uncertainties $U_{j,g}(x_l)$. In order to have a reasonable computing time during traffic simulation, the number of samples of $Q_j(x_l)$ is limited to $n_{SP} = 1,000$. Gathering the 24 internal forces, $1,000$ candidate-model samples and the two traffic lanes, the number of influence lines to be processed during traffic simulations is $48,000$.

The modeling uncertainties $U_{j,g}(x_l)$ are presented in Table 1. Model simplifications, mesh refinement and additional uncertainty are sources whose PDF is estimated based on engineering judgment and have identical distributions over x_l. Influence-line interpolation error is considered as a bias that is added to each candidate-model sample such that no PDF is estimated. The other sources of uncertainty represent parameters with secondary influence on the structural response and their effect on the model predictions is propagated through the finite-element model using a thousand Monte-Carlo simulations. Except for the interpolation error, all other sources of modeling uncertainty were also used for defining the threshold bounds during model falsification and in Pasquier et al. (2014).

For example, Figure 7 presents the combined parameter and modeling uncertainty associated with influence lines of internal forces $N_{ch,s1}$ and $M_{ch,s1}$ for the initial model set (IMS) and the candidate model set (CMS). At the maximum axial force and moment, the IMS uncertainty ranges from 192 to 231 kN and from 2.86 to 3.78 kNm as the CMS uncertainty ranges from 208 to 230 kN for the axial force and from 3.07 to 3.54 kNm for the moment. A reduction of uncertainty is observed between the IMS and CMS uncertainty due to the falsification of inadequate model instances by the measurements.

Traffic simulations and hot-spot stress-range calculation

Traffic simulations are based on 18 days of continuous traffic measurements on the bridge with mobile WIM device "Golden River". WIM raw data contain information on VAT, VS, GVW, TVL, AVW, AVS of heavy vehicles crossing the bridge on the west lane (direction Aarwangen) and on the east lane (direction Niederbipp) during the period from 9/10/1998 to 27/10/1998. A total number of $6,577$ heavy vehicles ($3,655$ vehicles on the west lane, $2,922$ vehicles on the east lane) are classified using the traffic simulation tool presented in section "Traffic model". For each class, the multivariate vector $[GVW, TVL, AVW, AVS]$ is described by a mean vector and a covariance matrix. PDFs for VS and VIT are fitted based on the WIM data. Table 2 summarizes their PDFs depending on whether heavy-vehicle traffic crosses bridge west lane or east lane. Once the traffic on the two lanes has been completely defined, random sequences of weekly axle loadings of west

and east lanes are generated for each of n_{SP} candidate-model samples. Spectra of internal forces are determined by superimposing traffic axle-loading samples to the influence lines of N, V and M.

From the internal-force spectra, nominal-stress spectra are calculated at each time t using Eq. (6). In this expression, A and W are random variables due to the member geometrical uncertainty. Their values vary in relation with diameter and thickness uncertainty displayed in Table 1.

The SCF values are determined by linear interpolation (and occasionally extrapolation) of K-joint SCF table at hot spot 1 obtained experimentally and numerically by Schumacher et al. (2003) on similar joint geometry. The interpolation is based on the non-dimensional parameters of the joints ($\beta = 0.48$, $\gamma = 4.06$ and $\tau = 0.4$) for brace angles $\theta = 45$. The SCF values that are displayed in Table 3 are used to calculate the hot-spot stress spectra at $hs1$ based on Eq. (8). The hot-spot stress spectra are then transformed into hot-spot stress-range histograms using the rainflow algorithm.

Remaining-fatigue-life evaluation

The remaining fatigue lives of the four joints are calculated by comparing the hot-spot stress-range histograms to $\mathrm{S_{rhs}}$-N curves. For this study, 30 experimental data points (Acevedo and Nussbaumer 2012; Zamiri 2014) are used to build a regression model. This model is a Gaussian function $\mathcal{N}(a + b \cdot \log(\Delta\sigma_{hs}), c^2)$ with $[a, b, c] \sim \mathcal{N}(\mu, \Sigma)$ and

$$\mu = [26.88, -2.61, -0.90]^T, \quad \Sigma = \begin{bmatrix} 1.71 & -0.34 & 0 \\ -034 & 0.07 & 0 \\ 0 & 0 & 0.02 \end{bmatrix}$$

where a and b are parameters of the straight line representing the mean value of the regression model and having standard deviation c. In addition, $[a, b, c]$ are random variables that are described by a multivariate Gaussian distribution of parameters μ and Σ. The latter includes variances and correlation values of $[a, b, c]$.

In order to be comparable with experimental data that were obtained with various chord thick-

nesses, hot-spot stress-range resistances S_{rhs} and hot-spot stress ranges $\Delta\sigma_{hs}$ obtained from traffic simulation are corrected to refer to stress resistance of 20 mm thickness members $S_{rhs,20}$ using Eq. (12), given by Schumacher et al. (2003).

$$S_{rhs,20} = \left(\frac{T}{20}\right)^{0.25} \cdot S_{rhs,T}, \quad \forall T > 20\,mm \tag{12}$$

In Eq. (12), $S_{rhs,T}$ refers to the hot-spot stress range of a joint having a chord thickness of T. For the joints under study, the chord thickness is $T = 50$ mm. This fatigue model does not consider a fatigue limit for the low stress ranges. The fatigue limit implies that low stress-range values lead to an infinite number of cycles, i.e. no damage is induced when no cycles are greater than the limit. Since the purpose of this study is to determine the remaining-fatigue-life distribution, a continuous $\mathrm{S_{rhs}}$-N curve is thus preferred, which is a strong but conservative assumption.

The hot-spot stress-range histograms are compared to this regression model in order to obtain the number of cycles and compute the damage index using Eq. (9). The process is repeated randomly $n_{SN} = 1,000$ times until convergence of the damage-index distribution is achieved. This repeated process is necessary since $n_{SP} = 1,000$ samples of stress-range histograms are insufficient to capture the $\mathrm{S_{rhs}}$-N curve uncertainty associated with the regression model. Finally, the remaining fatigue life of each candidate-model sample is calculated using Eq. (10), with $R_{\mathrm{year}} = 1/52$ since one week of traffic is simulated, in order to determine the distribution of RFL_j for each critical joint. This distribution is composed of $n_{SP} \times n_{SN} = 1,000,000$ samples. The convergence of the distribution is verified with a lower value of n_{SP} in order to ensure the correctness of the repeated $\mathrm{S_{rhs}}$-N curve comparison process. Based on the distribution of RFL_j, prediction thresholds are determined using a target reliability $\phi_p = 0.95$. Since the identification reliability is $\phi_d = 0.95$, the probability of having the true prediction value included between threshold bounds for each critical joint independently is at least $\phi_d \cdot \phi_p = 0.90$.

Figure 8 presents the remaining-fatigue-life predictions that are determined using the population-based prognosis methodology for the four critical joints (see Figure 5). A second axis represents

406 the results in term of equivalent number of trucks crossing the bridge in both directions during
407 life time. This figure compares predictions made with the initial population of model instances
408 (IMS), the candidate model set (CMS) and a design model that is composed of pinned-truss con-
409 nections without expansion joints and design values for Young's moduli of steel (210 GPa) and
410 concrete (35 GPa). The design-model remaining fatigue life is calculated using prescriptions of
411 Zhao et al. (2000) for the internal-force determination and the same random process for traffic and
412 remaining-fatigue-life computation as for IMS and CMS predictions. For the CMS predictions,
413 the value displayed in Figure 8 is the lower bound of the confidence intervals including 95% of the
414 probability distribution. This value is important since it expresses the lowest acceptable value for
415 the remaining-fatigue-life prediction. Uncertainty reduction between IMS and CMS predictions is
416 computed based on the percentage of reduction between IMS and CMS ranges defined as the dif-
417 ference of upper and lower prediction thresholds. The improvement ratio is obtained by comparing
418 the design-model prediction and the CMS lower threshold. The RFL values that are found are very
419 high and would be reduced with higher traffic loads. However, this allows for relative comparison
420 of design-model prediction and CMS predictions. Note that since a single slope $\mathrm{S_{rhs}}$-N curve re-
421 sistance model is used, it is expected that many model instances would lead to an infinite life using
422 a fatigue limit.

423 These results reveal an uncertainty reduction of up to 57% of the reserve-capacity predictions
424 for joint 1-south and joint 2-north. In addition, when compared with the design-model predictions,
425 the candidate-model-prediction lower bounds depict an improvement of remaining fatigue life up
426 to 170% for joint 2-south. This means that the use of data interpretation combined with an en-
427 hanced finite-element analysis lead to less conservative estimates of the fatigue reserve capacity.
428 This observation was also made by Pasquier et al. (2014). In addition, this second study of the
429 Aarwangen Bridge confirms the good condition of the four tubular joints, whose reserve capacity
430 against fatigue failure is much longer than the bridge service life.

Relative importance of uncertainty sources

The relative importance is determined using the response-surface method. Sources such as parameter uncertainty, modeling uncertainty, traffic uncertainty and $\mathrm{S_{rhs}}$-N curve uncertainty are varied individually through the Monte-Carlo process while having the other sources constant in order to determine the distribution of X_i (Eq. 11). This type of sensitivity analysis is local, i.e. it accounts for individual parameter variability and its effect on the model response. Then, using the same random samples, all sources are varied to determine Y_i. Finally, the relative importance is obtained as presented in Figure 9. This bar diagram describes the relative importance of each uncertainty source on the remaining fatigue life for the four critical joints before data interpretation is undertaken. The traffic uncertainty is the main uncertainty source related to the reserve fatigue capacity, with 60 to 78% of relative importance between the joints. The second source is the parameter uncertainty, with 18 to 38% influence depending on the joints. Modeling uncertainty (see Table 1) and uncertainty associated with $\mathrm{S_{rhs}}$-N curve regression model have very low influences on remaining-fatigue-life predictions.

The parameter-uncertainty relative importance is composed of the relative importance of individual model parameters $\boldsymbol{\theta}$. Figure 10 displays their relative importance on the remaining-fatigue-life predictions. The stiffness of the southern expansion joint and the rotational stiffness of truss connections are shown to be the most influential depending on the critical joint location. The southern expansion joint has more importance than the northern expansion joint since the four critical joints are located on the bridge southern span. In addition, the material Young's moduli have a minor influence on predictions, particularly the steel Young's modulus that has the lowest influence. This shows that modeling assumptions associated with boundary conditions and connection stiffnesses are important for the accuracy of fatigue assessments. These structural components are usually the main sources of systematic errors in the modeling of complex structures such as the Aarwangen Bridge. Therefore, special care is required when modeling such components.

The comparison of uncertainty source importance is also carried out after data interpretation as shown in Figure 11. In this case, model falsification impacts only the parameter uncertainty

that is greatly reduced as presented already in Figure 8. Here, the relative importance of parameter uncertainty is decreased to the level of modeling uncertainty and S_{rhs}-N curve uncertainty. Consequently, traffic uncertainty has the dominant influence.

In Figures 9 and 11, the uncertainties associated with the traffic model have a high influence on remaining-fatigue-life values. This is due to the large variability of truck weights in the simulated traffic, particularly the part of trucks with lower weight, that lead to large variability in the number of stress ranges and, subsequently, to large variability in remaining fatigue life. Such light-truck traffic is not of main concern since the most important value is the lower bound of the remaining-fatigue-life prediction. However, traffic uncertainty could be reduced by using more accurate WIM data during a longer period. Furthermore, this would allow for the consideration of traffic increase (weights and volume) over time, which is a parameter that is not taken into account in this study. The Aarwangen Bridge study also shows that the uncertainty associated with fatigue models is not significant when including the traffic and model-parameter uncertainty.

DISCUSSION

The study of the Aarwangen Bridge using the population-based prognosis methodology reveals satisfactory fatigue resistance of the four critical joints. Although a constant traffic scenario is assumed, a traffic increase could be taken into account in order to consider a heavy-vehicle loading increase. Since traffic evolution is unknown, this uncertainty could be taken into account in the methodology, and this would increase the uncertainty related to remaining-fatigue-life predictions. This uncertainty increase may also be reduced by investing further in the determination of real traffic on bridges for longer periods.

The four joints under study would have a sufficient reserve capacity using design-model predictions. Considering the design service life of 70 years (based on SIA261 Code (2003)), predicting either 400 years or $1,200$ years has the same impact on decision making related to retrofitting these joints. In practice, the fatigue assessment of an existing bridge starts by using conservative and simplified models prior to more advanced evaluations (see Figure 12). Population-based prognoses become beneficial when design-model predictions are below the required service lives

and imply intervention. In such situations, model-based data interpretation provide a more sophisticated approach for refining fatigue assessment. First, data interpretation is combined with traffic-load model and S-N curve from codes as it was proposed for the Aarwangen Bridge in Pasquier et al. (2014). If performance evaluations lead to intervention necessity, traffic-load models based on WIM data and advanced fatigue models are used to further increase the refinement of the fatigue assessment. If the performance is still not satisfactory, interventions are unavoidable. Based on this framework, improvements of 170% in the remaining-fatigue-life prediction, as this is determined for the Aarwangen Bridge, compared with design-model predictions that would be below the required service lives, would be economically and environmentally significant. Note that the process presented in Figure 12 is purposely compatible with AASHTO (2008) that recommends progressive levels of sophistication including advanced analysis, WIM study and variability of fatigue resistance.

Sensitivity analysis shows that traffic uncertainty and model-parameter uncertainty are the most important. It should be noted that the extent of traffic uncertainty is not high enough to overwhelm the model-parameter uncertainty. Due to the reduction of uncertainty associated with the physical parameters using data interpretation, a significant reduction in remaining-fatigue-life predictions is observed. In addition, the uncertainty associated with structural components such as boundary conditions and connection stiffnesses is important when evaluating the fatigue reserve capacity. Special care is thus required when modeling such components. In addition, uncertainties associated with the hot-spot method, including the determination of SCF factors (Table 3) and the thickness correction (Eq. 12), are not explicitly included. If one has the possibility to estimate them, these uncertainties can be accommodated by the methodology. The approach recommended by Schumacher et al. (2003) was preferred over the original proposed by Gurney (1977). Note that the uncertainty related to Eq. (12) is included implicitly in $\mathrm{S_{rhs}}$-N curve definition.

This methodology is not intended to be more accurate than direct field observations and specific modeling of the joints to determine the remaining fatigue life. However, the number of joints, especially the number of hot-spot locations, that can be monitored and modeled are limited in

practice. In this context, physics-based models are required to predict stresses and fatigue behavior at unmeasured locations. Populations of candidate models are less conservative than current design models and this paper demonstrates that such populations can be accommodated with advanced traffic-load and fatigue-damage models. Nevertheless, future work may include comparison of the predictions with field observations in order to evaluate the accuracy of the methodology.

This methodology is adaptable for other hot-spot locations and other types of joints and also for studying fatigue-strength globally. Extraction of internal forces from the finite-element model at more locations for influence-line calculations would not lead to additional computing time. Conversely, traffic simulations would be more time consuming with the increase in the number of joints. However, since the algorithm has a linear computational complexity, this task may be computationally feasible using parallel computing. In addition, another development would be the inversion of this methodology into a measurement-system design approach that would determine optimal measurement locations either maximizing the lower bound of remaining-fatigue-life predictions or minimizing uncertainty related to remaining-fatigue-life predictions.

CONCLUSION

This paper presents an enhanced methodology for improving remaining-fatigue-life evaluations of existing bridges using data interpretation, traffic simulations and hot-spot fatigue evaluations that extends work from Pasquier et al. (2014). A full-scale bridge study is carried out to illustrate the benefits of this methodology and the relative influence of uncertainties associated with remaining-fatigue-life predictions. The following conclusions are made:

- The population-based prognosis reduces uncertainty associated with the fatigue reserve capacity evaluation, and provides less conservative estimations of remaining-fatigue-life predictions than standard design procedures. Furthermore the methodology proposed in this paper is less conservative than that proposed by Pasquier et al. (2014).
- This methodology allows for the propagation of uncertainty associated with remaining-fatigue-life prognosis (finite-element, traffic and fatigue damage) and thus provides support

for structural management decisions related to retrofit, repair and replacement.

- Traffic models and structural model parameters are the most important sources of uncertainties for predicting the remaining fatigue life of K-joint tubular structures. While fatigue life might be influenced by other uncertainties, such as those associated with weld geometry and residual stresses, these aspects are difficult to quantify and control. The use of the S_{rhs}-N curve for hollow sections along with its thickness correction in Eq. 12 is assumed to provide a conservative bound for these effects.

ACKNOWLEDGEMENTS

This work was funded by the Swiss National Science Foundation under Contract no. 200020-155972.

REFERENCES

References

AASHTO (2007). *LRFD Bridge Design Specifications, 4th Edition*. American Association of State Highway and Transportation Officials, Washington, DC.

AASHTO (2008). "Manual for bridge evaluation.

Acevedo, C. and Nussbaumer, A. (2012). "Effect of tensile residual stresses on fatigue crack growth and S-N curves in tubular joints loaded in compression." *International Journal of Fatigue*, 36(1), 171–180.

Atamturktur, S., Liu, Z., and Cogan, S.and Juang, H. (2014). "Calibration of imprecise and inaccurate numerical models considering fidelity and robustness: a multi-objective optimization-based approach." *Structural and Multidisciplinary Optimization*, 1–13.

Beck, J. (2010). "Bayesian system identification based on probability logic." *Structural Control and Health Monitoring*, 17(7), 825–847.

Beck, J. and Au, S.-K. (2002). "Bayesian updating of structural models and reliability using Markov chain Monte Carlo simulation." *Journal of Engineering Mechanics*, 128(4), 380–391.

Beck, J. and Katafygiotis, L. (1998). "Updating models and their uncertainties. I: Bayesian statistical framework." *Journal of Engineering Mechanics*, 124(4), 455–461.

Beven, K. (2006). "A manifesto for the equifinality thesis." *Journal of Hydrology*, 320(1-2), 18–36.

Box, G. and Draper, N. (1959). "A basis for the selection of a response surface design." *Journal of the American Statistical Association*, 54(287), 622–654.

Brynjarsdóttir, J. and O'Hagan, A. (2014). "Learning about physical parameters: The importance of model discrepancy." *Inverse Problems*, 30(11), 114007.

Crespo-Minguillón, C. and Casas, J. (1997). "A comprehensive traffic load model for bridge safety checking." *Structural Safety*, 19(4), 339–359.

Downing, S. and Socie, D. (1982). "Simple rainflow counting algorithms." *International Journal of Fatigue*, 4(1), 31–40.

EN1993-1-9 (2005). *Eurocode 3 - Design of steel structrures - Part 1-9: Fatigue*. European committee for standardization.

Fang, H., Rais-Rohani, M., Liu, Z., and Horstemeyer, M. (2005). "A comparative study of metamodeling methods for multiobjective crashworthiness optimization." *Computers & Structures*, 83(25), 2121–2136.

Farajpour, I. and Atamturktur, S. (2012). "Error and uncertainty analysis of inexact and imprecise computer models." *Journal of Computing in Civil Engineering*, 27(4), 407–418.

Goulet, J.-A. and Smith, I. (2013). "Structural identification with systematic errors and unknown uncertainty dependencies." *Computers & Structures*, 128, 251–258.

Guo, T., Frangopol, D., and Chen, Y.-W. (2012). "Fatigue reliability assessment of steel bridge details integrating weigh-in-motion data and probabilistic finite element analysis." *Computers & Structures*, 112, 245–257.

Gurney, T. (1977). *Theoretical analysis of the influence of toe defects on the fatigue strength of fillet welded joints*. Welding Institute.

Hobbacher, A. (2007). "Recommendations for fatigue design of welded joints and components, IIW document XIII-1251-07 / XV-1254-07." *International institute of welding*.

Kleiber, C. and Kotz, S. (2003). *Statistical size distributions in economics and actuarial sciences*, Vol. 470. John Wiley & Sons.

Kwon, K., Frangopol, D., and Kim, S. (2013). "Fatigue performance assessment and service life prediction of high-speed ship structures based on probabilistic lifetime sea loads." *Structure and Infrastructure Engineering*, 9(2), 102–115.

Leahy, C., OBrien, E., Enright, B., and Hajializadeh, D. (2014). "Review of HL-93 bridge traffic load model using an extensive WIM database." *Journal of Bridge Engineering*, in press, 04014115.

Leander, J., Andersson, A., and Karoumi, R. (2010). "Monitoring and enhanced fatigue evaluation of a steel railway bridge." *Engineering Structures*, 32(3), 854–863.

Leitão, F., Da Silva, J., da S Vellasco, P., De Andrade, S., and De Lima, L. (2011). "Composite (steel–concrete) highway bridge fatigue assessment." *Journal of Constructional Steel Research*, 67(1), 14–24.

Li, Z., Chan, T., and Ko, J. (2001). "Fatigue damage model for bridge under traffic loading: application made to Tsing Ma Bridge." *Theoretical and Applied Fracture Mechanics*, 35(1), 81–91.

600 Liu, M., Frangopol, D., and Kwon, K. (2010). "Fatigue reliability assessment of retrofitted steel bridges integrating
601 monitored data." *Structural Safety*, 32(1), 77–89.
602 Mackay, D. (2003). *Information theory, inference and learning algorithms*. Cambridge University Press.
603 Maddox, S. (1997). "Developments in fatigue design codes and fitness-for-service assessment methods." *Proceed-*
604 *ings IIW International Conference on Performance of Dynamically Loaded Welded Structures*, Welding Research
605 Council, New York.
606 Meystre, T. and Hirt, M. (2006). "Evaluation de ponts routiers existants avec un modèle de charge de trafic actualisé,
607 Mandat de recherche AGB 2002/005.
608 Miner, M. (1945). "Cumulative fatigue damage." *ASME Journal of Applied Materials*, 12, A159–A164.
609 Morales-Nápoles, O. and Steenbergen, R. (2015). "Large-scale hybrid Bayesian network for traffic load modeling
610 from weigh-in-motion system data." *Journal of Bridge Engineering*, 20(1), 04014059.
611 Moses, F., Schilling, C. G., and Raju, K. (1987). *Fatigue evaluation procedures for steel bridges*. Number 299.
612 Neumann, M. and Gujer, W. (2008). "Underestimation of uncertainty in statistical regression of environmental models:
613 influence of model structure uncertainty." *Environmental Science & Technology*, 42(11), 4037–4043.
614 Niemi, E., Fricke, W., and Maddox, S. (2006). "Fatigue analysis of welded components, designer's guide to the
615 structural hot-spot stress approach, IIW-1430-00." *International Institute of Welding*.
616 Papadimitriou, C., Beck, J., and Katafygiotis, L. (2001). "Updating robust reliability using structural test data." *Prob-*
617 *abilistic Engineering Mechanics*, 16(2), 103–113.
618 Pasquier, R., Goulet, J.-A., Acevedo, C., and Smith, I. (2014). "Improving fatigue evaluations of structures using
619 in-service behavior measurement data." *Journal of Bridge Engineering*, 19 (11), 04014045.
620 Schumacher, A., Sturm, S., Walbridge, S., Nussbaumer, A., and Hirt, M. (2003). "Fatigue design of bridges with
621 welded circular hollow sections." *Report ICOM 489E*, Swiss Federal Institute of Technology (EPFL), Lausanne.
622 SIA261 Code (2003). *Norme SIA 261: Actions on Structures*. SIA Zurich.
623 SIA263 Code (2003). *Norme SIA 263 : Steel structures*. SIA Zurich.
624 Siriwardane, S., Ohga, M., Dissanayake, R., and Taniwaki, K. (2008). "Application of new damage indicator-based
625 sequential law for remaining fatigue life estimation of railway bridges." *Journal of Constructional Steel Research*,
626 64(2), 228–237.
627 Soliman, M., Frangopol, D., and Kown, K. (2013). "Fatigue assessment and service life prediction of existing steel
628 bridges by integrating SHM into a probabilistic bilinear S-N approach." *Journal of Structural Engineering*, 139(10),
629 1728–1740.
630 Sweeney, R. (1976). "The load spectrum for the Fraser River Bridge at New Westminster, BC." *Presented at the 75th*
631 *Technical Conference, AREA, Chicago, Illinois*, Vol. 77.
632 Yuen, K.-V. (2010). *Bayesian methods for structural dynamics and civil engineering*. Wiley.

633 Zamiri, F. (2014). “Welding simulation and fatigue assessment of tubular K-joints in high-strength steel.” Ph.D. thesis,
634 # 6158, Swiss Federal Institute of Technology (EPFL), # 6158, Swiss Federal Institute of Technology (EPFL).
635 Zhang, J., Wan, C., and Sato, T. (2013). “Advanced Markov chain Monte Carlo approach for finite element calibration
636 under uncertainty.” *Computer-Aided Civil and Infrastructure Engineering*, 28(7), 522–530.
637 Zhao, X., Herion, S., Packer, J., et al. (2000). “Design guide for circular and rectangular hollow section joints under
638 fatigue loading.” *CIDECT: Comité international pour le développement et l’étude de la construction tubulaire 8*,
639 TüV-Verlag Rheinland, Köln.
640 Zhou, Y. (2006). “Assessment of bridge remaining fatigue life through field strain measurement.” *Journal of Bridge*
641 *Engineering*, 11(6), 737–744.

Table 1. Sources and probability density functions of modeling uncertainties involved in influence-line prediction

Uncertainty source	Unit	PDF	Mean/Min	STD/Max
Model simplifications and FEM	%	Uniform	0	5
Additional uncertainty	%	Uniform	-1	1
Mesh refinement	%	Uniform	-2	0
Influence-line interpolation error	%	-	-0.36[a]	1.6[a]
Δv Poisson's ratio of concrete	-	Gaussian	0.19	0.025
Δt_1 steel profile thickness	%	Uniform	-10	10
Δt_2 steel profile thickness	%	Uniform	-12.5	12.5
ΔD_1 steel profile diameter	%	Uniform	-1	1
ΔD_2 steel profile diameter	%	Uniform	-1	1
Δt pavement thickness	%	Gaussian	0	2.5

[a]Minimum and maximum values of error from x_1 to x_{193} for $N_{ch,s1}$.

Table 2. Probability density functions of vehicle speeds and vehicle inter-arrival time included in the traffic model

	VS [km/h]	VIT [sec]
West lane	$\sim \mathcal{N}(50.15, 5.95)$	$\sim Burr(132.56, 1.10, 1.21)$[a]
East lane	$\sim \mathcal{N}(50.47, 6.66)$	$\sim Burr(154.60, 1.12, 1.13)$[a]

[a]Burr distribution are defined by three parameters: $Burr(\alpha, c, k)$.

Table 3. Values for the stress concentration factors SCF obtained according to Schumacher et al. 2003

SCF	Value [-]
$SCF_{i,ax-br}$	0.975
$SCF_{i,ipb1-br}$	0.52
$SCF_{i,ipb2-br}$	0.61
$SCF_{i,ax-ch}$	1.435
$SCF_{i,ipb-ch}$	1.51

Figure 1. Illustration of the calculation leading to the hot-spot stresses with the variables involved for a single joint j

Figure 2. Hot-spot location 1 on the critical joint

Figure 3. Methodology flowchart (Reference to equation numbers are given in parenthesis)

Figure 4. (a) Aarwangen Bridge model cross-section and (b) general overview [Reprinted from Pasquier et al. 2014]

Figure 5. Critical truss joint locations under study, focused on hot spot 1 [Adapted from Pasquier et al. 2014]

Figure 6. Uncertain model parameters [Adapted from Pasquier et al. 2014]

Figure 7. Combined parameter and modeling uncertainty associated with influence-line calculation of $N_{ch,s1}$ and $M_{ch,s1}$ for the initial model set (IMS) and the candidate model set (CMS)

Figure 8. Comparison of remaining-fatigue-life predictions with the initial model set (IMS), the candidate model set (CMS) and the design model for four critical joints using the population-based prognosis methodology

Figure 9. Relative importance of uncertainty sources on the remaining-fatigue-life predictions without data interpretation (IMS) for the four critical joints

Figure 10. Relative importance of model parameters θ on the remaining-fatigue-life predictions for the four critical joints

Figure 11. Relative importance of uncertainty sources on the remaining-fatigue-life predictions with data interpretation (CMS) for the four critical joints

Figure 12. Framework for the fatigue assessment of existing bridges

Figure 1

Click here to download Figure Fig_1.pdf

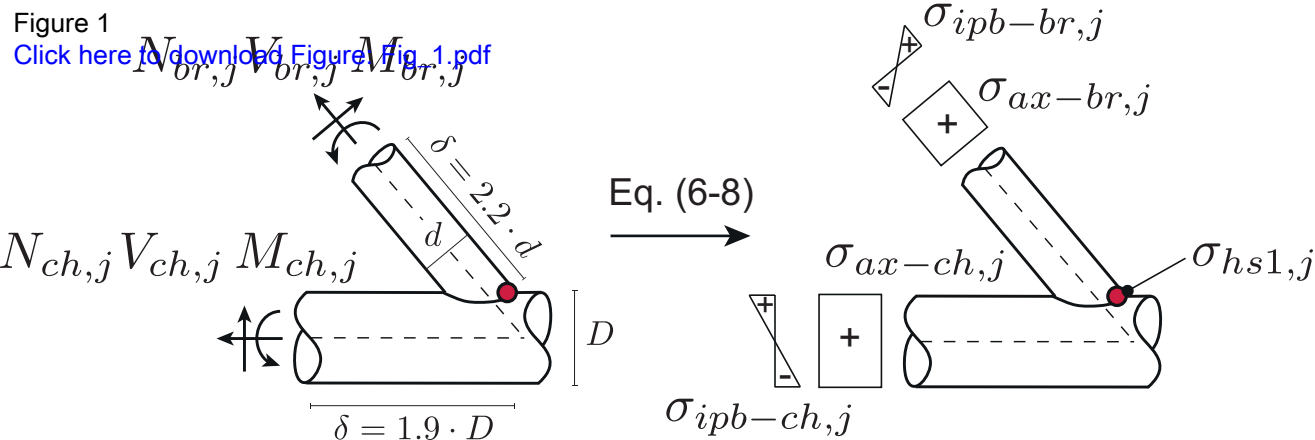

Figure 2

Click here to download Figure: Fig_2.pdf

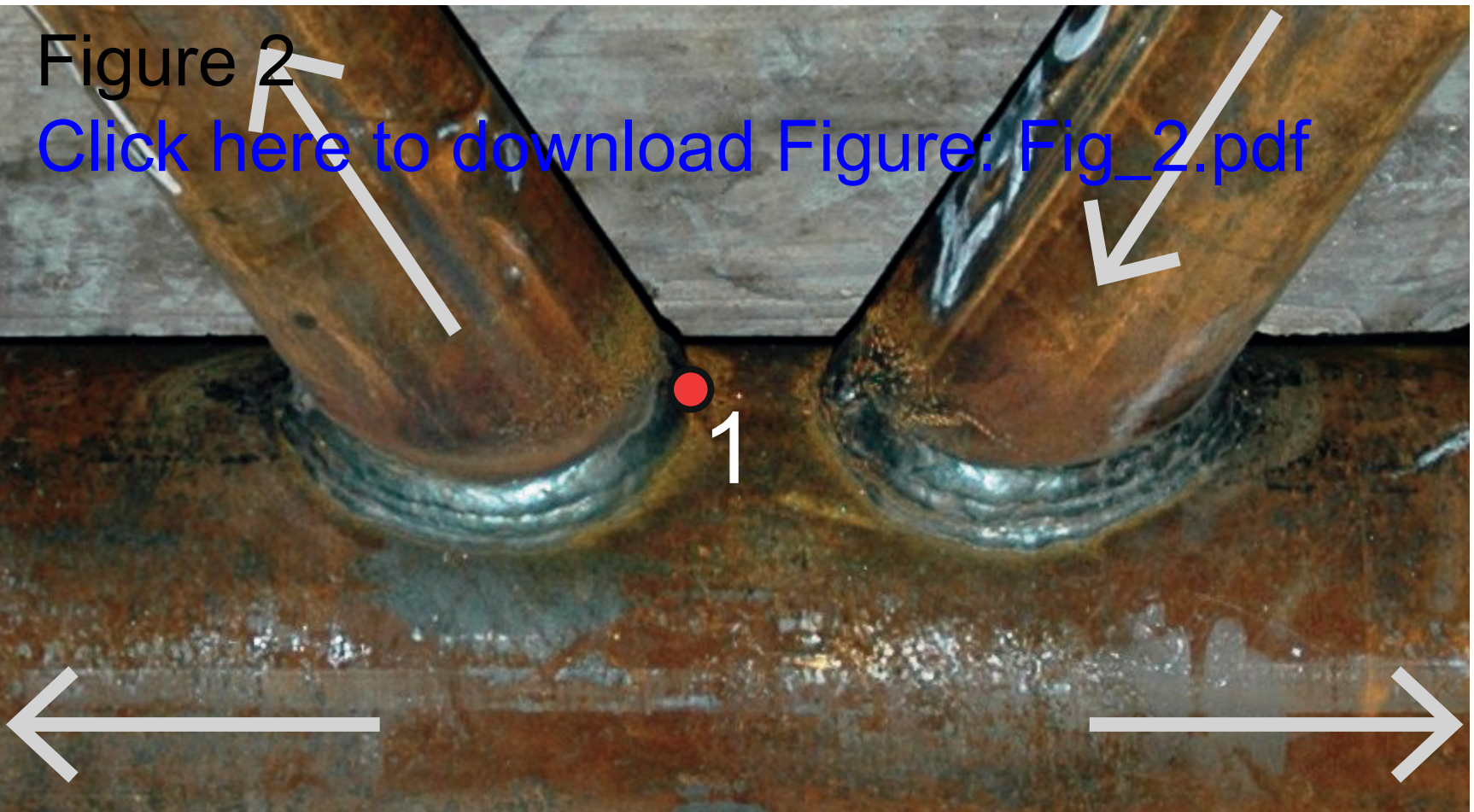

Figure 3
Click here to download Figure: Fig_3.pdf

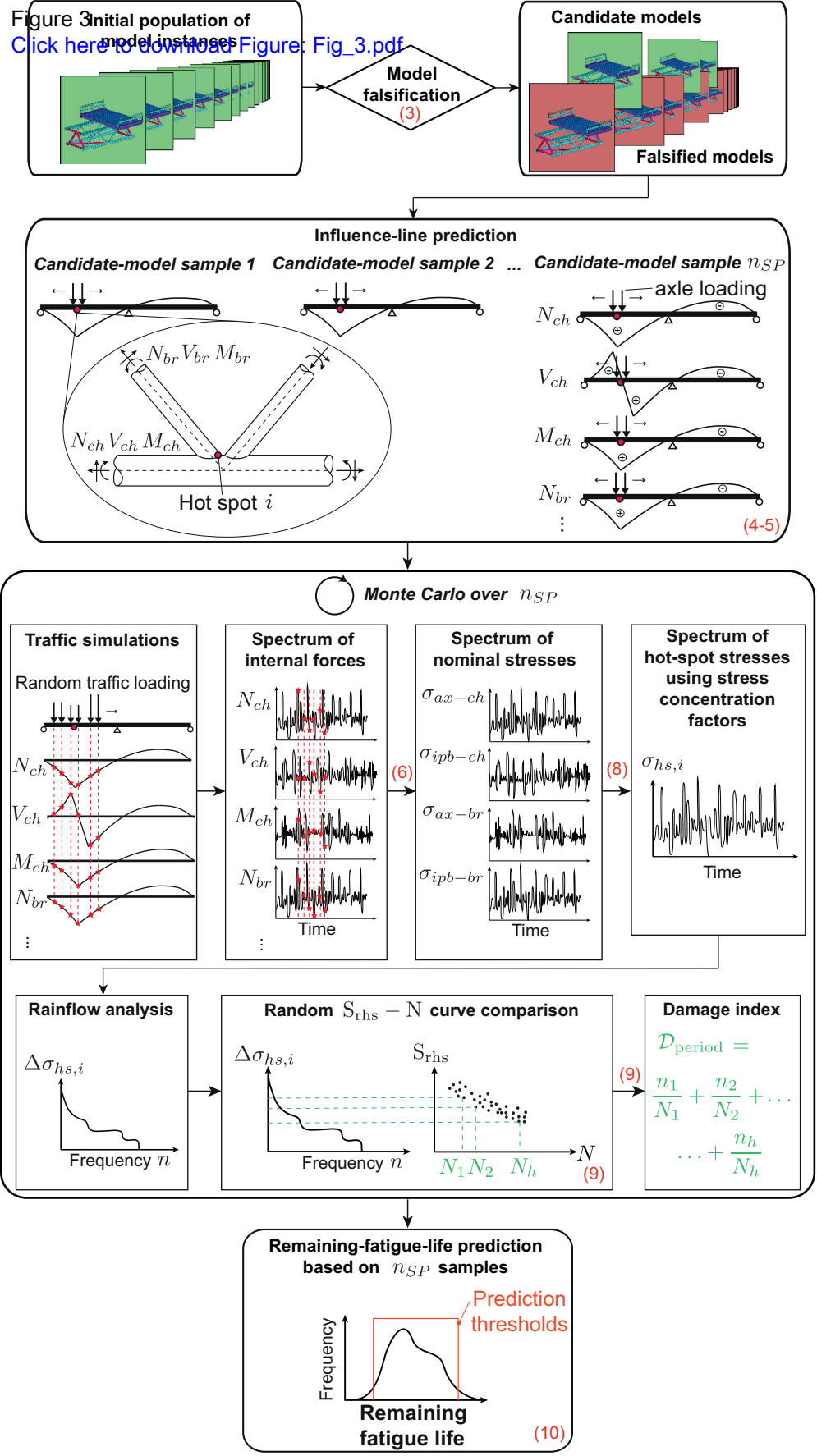

Figure 4

Click here to download Figure: Fig_4.pdf

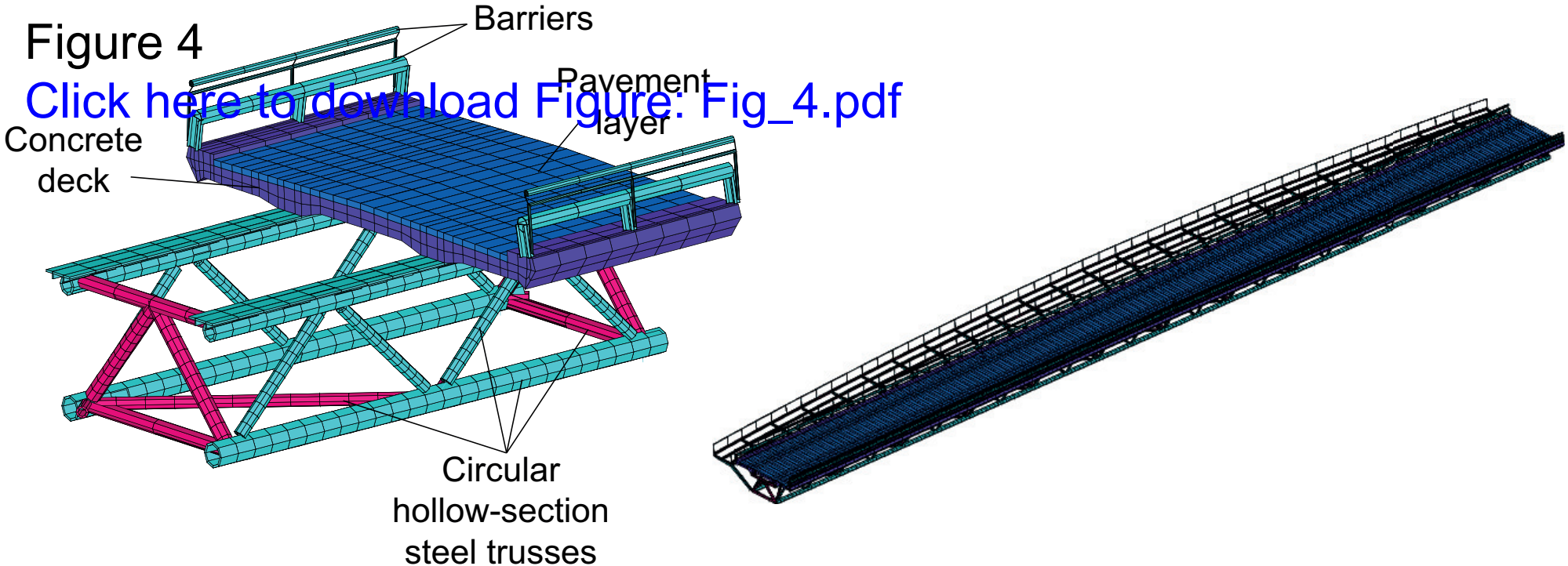

Figure 5

Click here to download Figure: Fig_5.pdf

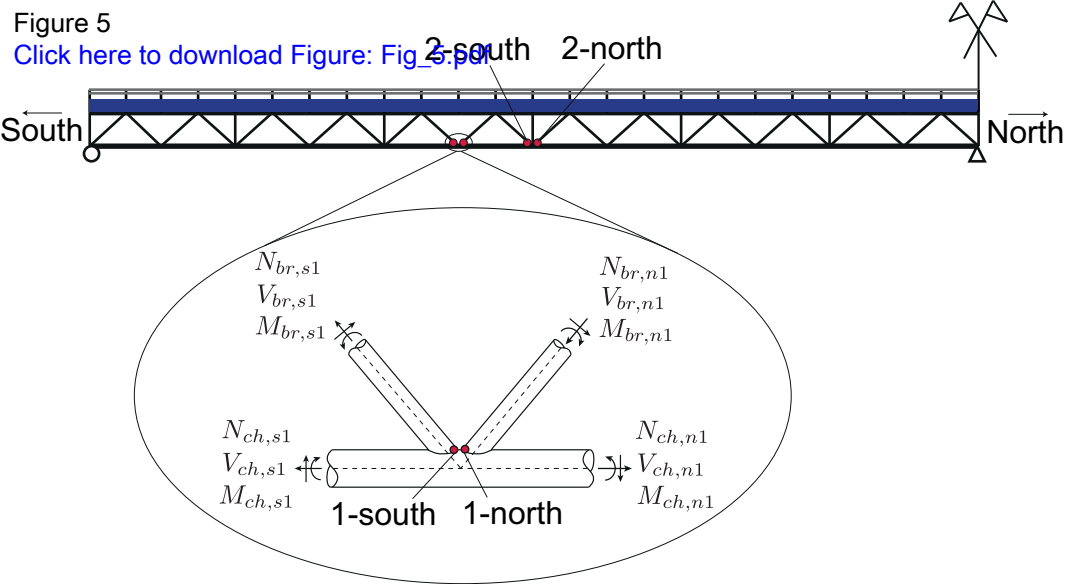

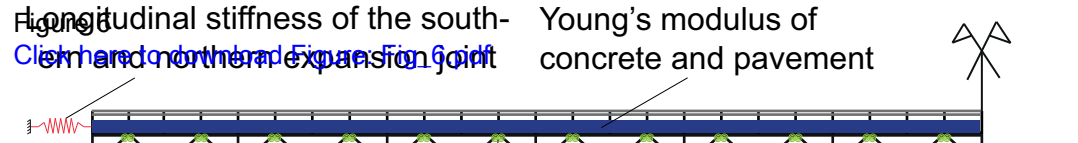
Figure 6
Click here to download Figure: Fig 6.pdf
Longitudinal stiffness of the south-ern and northern expansion joint
Young's modulus of concrete and pavement
South
North
Rotational stiffness of the truss connections
Young's modulus of steel

Figure 7
Click here to download Figure: Fig_7.pdf

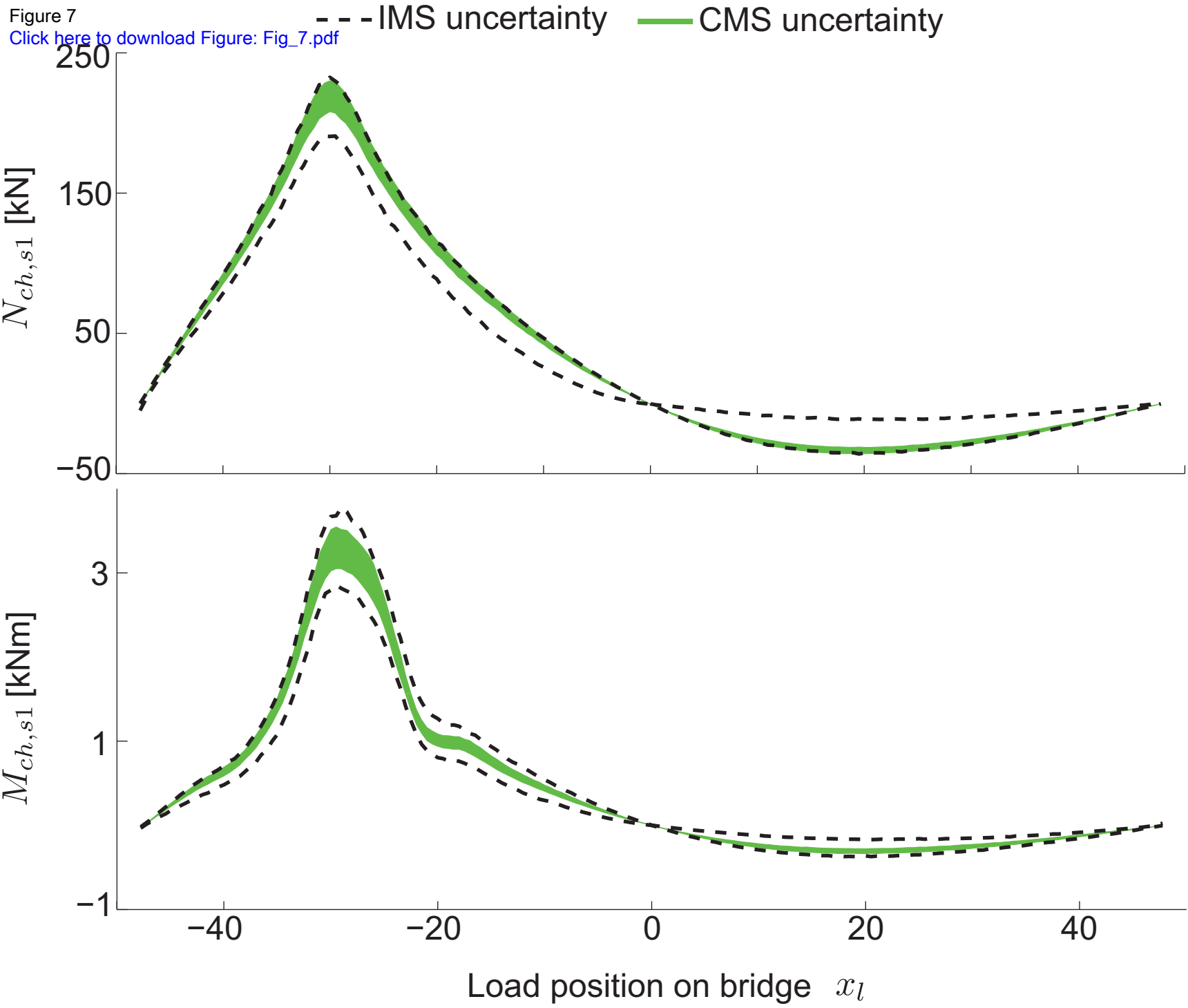

Figure 8 IMS-prediction distribution CMS-prediction thresholds Design-model prediction

Click here to download Figure: Fig_8.pdf

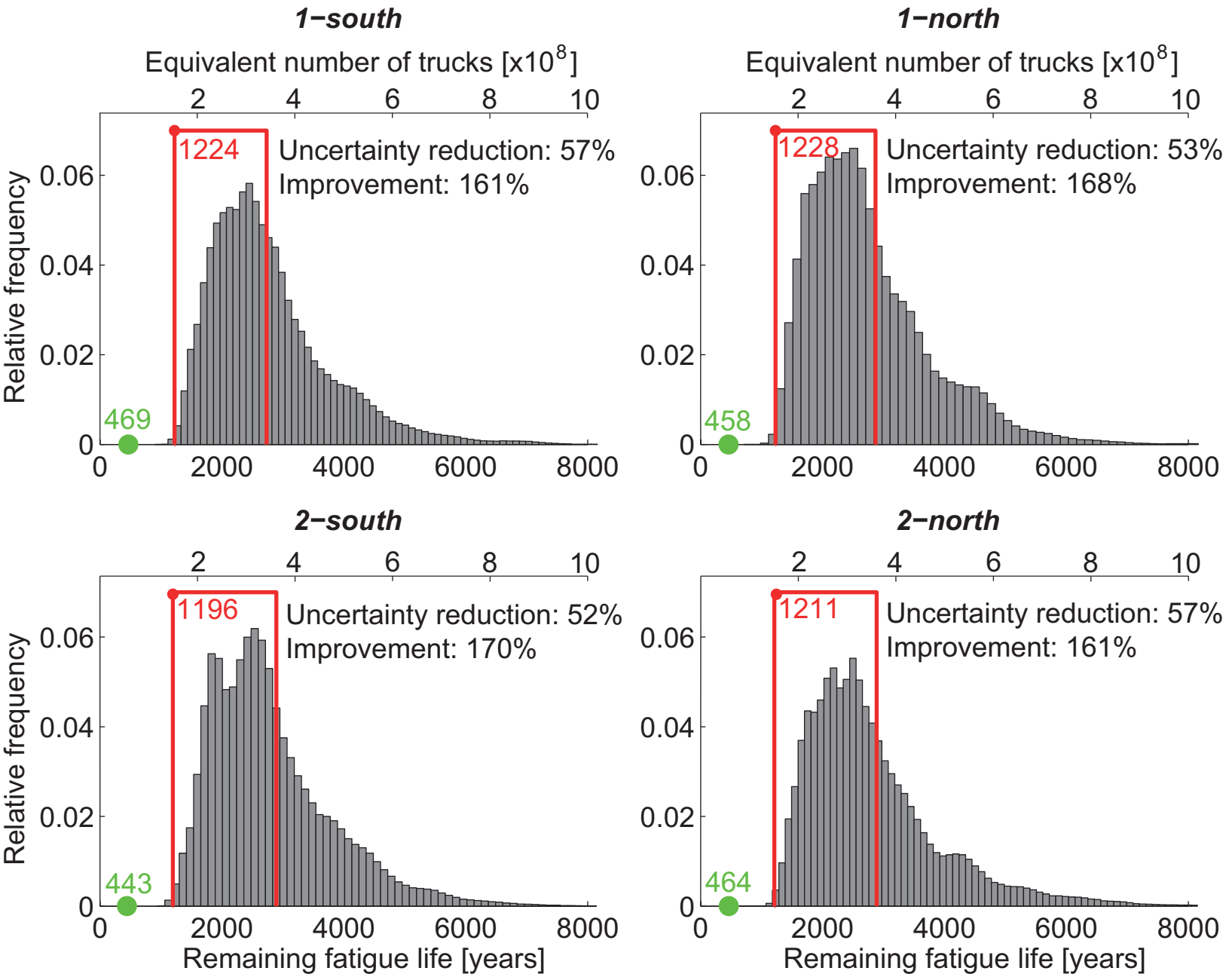

Figure 9
Click here to download Figure: Fig_9.pdf

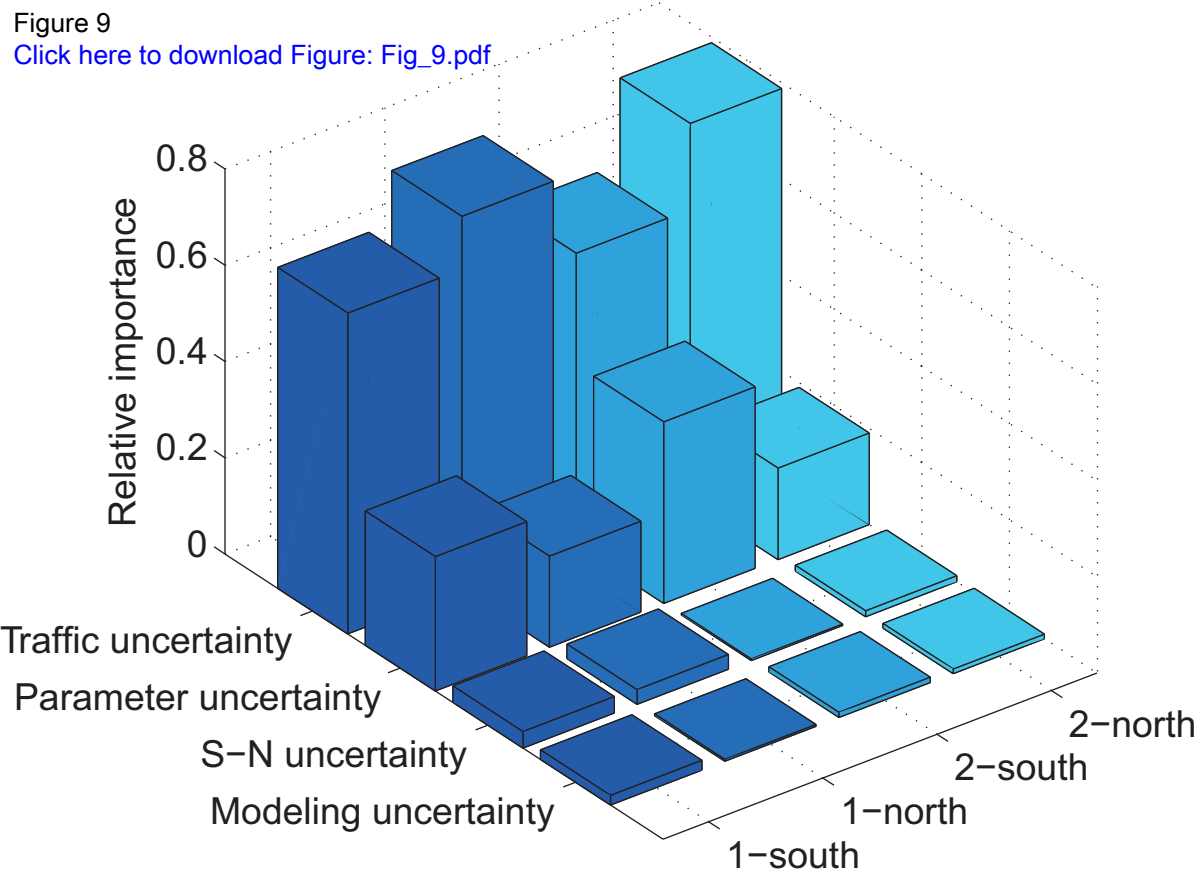

Figure 10

Click here to download Figure: Fig_10.pdf

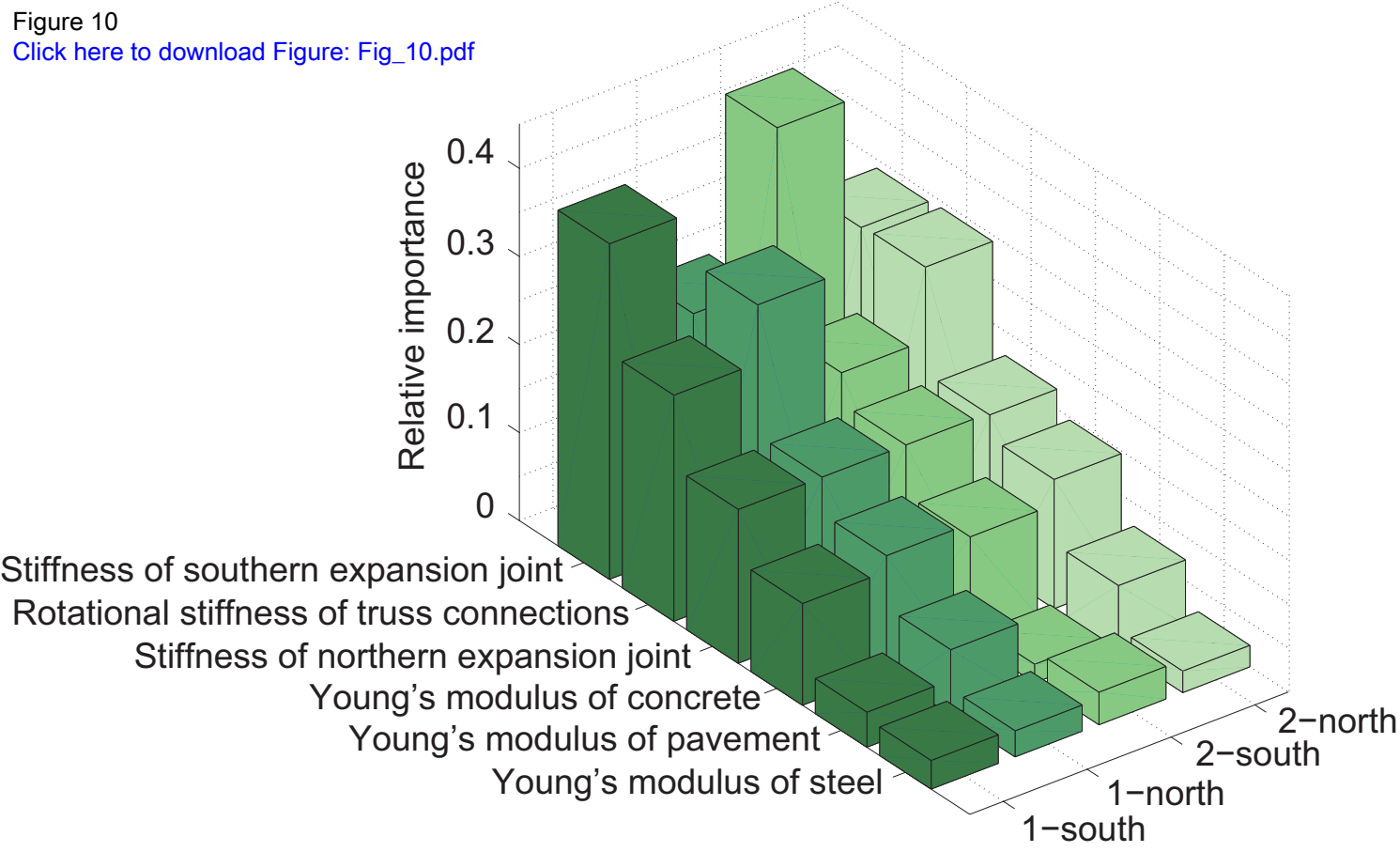

Figure 11

Click here to download Figure: Fig_11.pdf

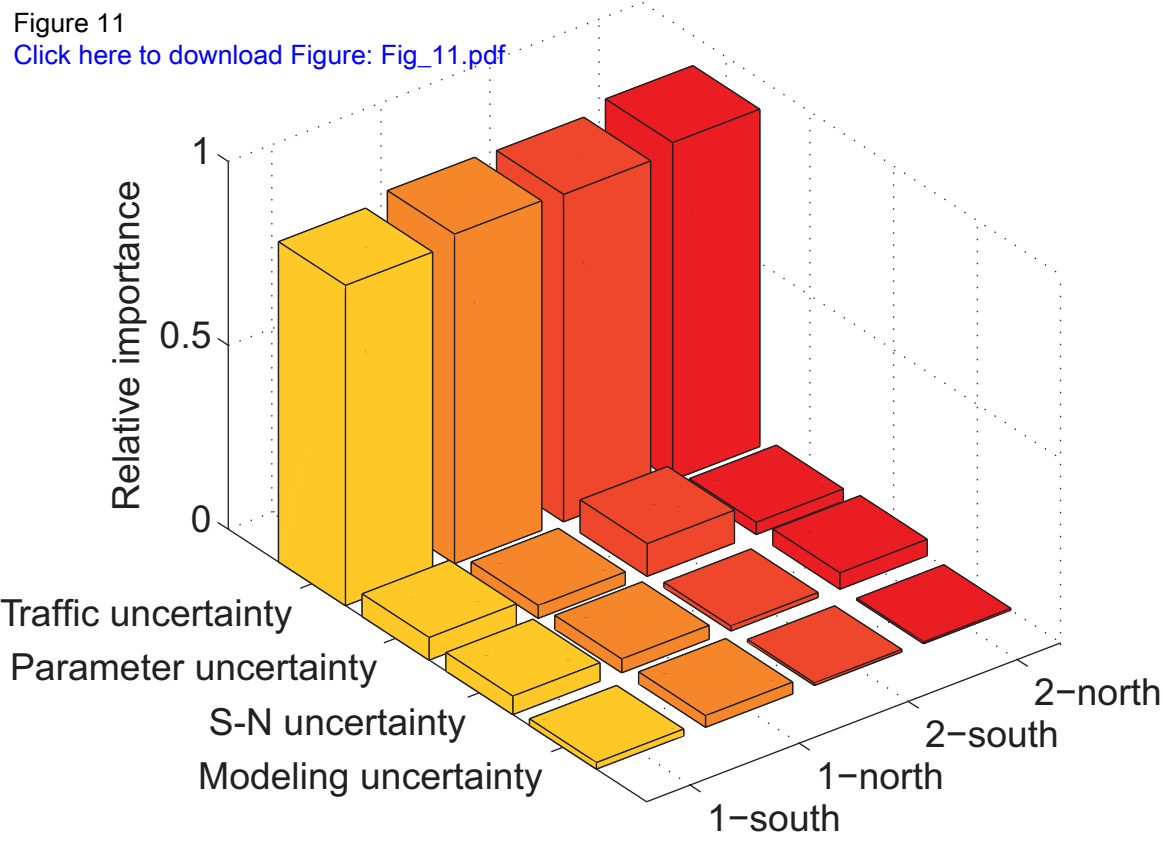

Figure 12

Click here to download Figure: Fig_12.pdf